Available online at www.sciencedirect.com
SCIENCE DIRECT®
Journal of Solid State Chemistry 177 (2004) 2903–2915
JOURNAL OF SOLID STATE CHEMISTRY
http://elsevier.com/locate/jssc

Optimizing Cs-exchange in titanosilicate with the mineral pharmacosiderite topology: framework substitution of Nb and Ge

Akhilesh Tripathi,[a] Dmitri G. Medvedev,[a,b] Jose Delgado,[a] and Abraham Clearfield[a,*]

[a] Department of Chemistry, Texas A&M University, P.O. Box 30012, College Station, TX 77842-3012, USA
[b] Department of Nuclear Engineering, Texas A&M University, College Station, TX 77843-3133, USA

Received 5 April 2004; received in revised form 18 April 2004; accepted 20 April 2004

Abstract

Titanosilicates with complete or partial substitution of Ge or Nb in the framework and having the mineral pharmacosiderite topology were hydrothermally prepared and their ion-exchange properties towards Cs were studied for Ti/Ge/Si, Ti/Si, Nb/Ti/Si and pure Ge phases. The basis for the differences in the ion exchange properties measured as distribution coefficients (K_d) for these materials are detailed via structural characterization using the Rietveld refinement technique on the X-ray powder diffraction data. The differences in affinity towards Cs^+ result either from the degree of hydration of the exchanger resulting in different coordination environments or the position of cesium ion in the eight-ring channel.

Keywords: Pharmacosiderite; Titanosilicate; Germanium; Niobium; Structure; Rietveld analysis; Ion exchange; Selectivity; Distribution constant; Cesium ion

1. Introduction

High radiation stability, resistance to chemical attack, compatibility with immobilization matrices, and extreme selectivity renders inorganic ion exchangers as useful materials for selective removal of radionuclides from highly alkaline liquid nuclear waste and their consequent safe storage [1–4].

We recently reported the results of our research correlating the ion-exchange properties of tunnel type titanium silicates for Cs^+ and Sr^{2+} with the coordination environment of these ions within the framework [5]. Pure and 25% Nb-substituted crystalline titanosilicates with the compositions $Na_2Ti_2O_3SiO_4{\cdot}2H_2O$ (TS) and $Na_{1.5}Nb_{0.5}Ti_{1.5}O_3SiO_4{\cdot}2H_2O$ (Nb–TS), respectively, and having the mineral sitinakite topology (referred to as CST for Crystalline SilicoTitanate in the literature), were prepared as a part of an ongoing collaboration with Westinghouse Savannah River Company, Sandia National Laboratories and the University of Notre Dame to develop inorganic ion exchangers suitable for the removal of ^{137}Cs and ^{90}Sr from tank wastes and to understand the origin of selectivity in them [6–8]. Among the two materials, Nb–TS demonstrated better Cs^+ removal whereas Sr^{2+} removal was more effective with pure TS. Structural studies carried out using the Rietveld analysis of powder diffraction data explained that a higher coordination environment of cesium in Nb–TS and strontium in TS is the main reason for the difference in the selectivity. The change in population of water vs. Na^+ in the eight-ring channels of Nb–TS due to Nb^{+5} substitution resulted in different hydration environments around Cs and Sr [5].

The synthetic titanosilicate analog of the mineral pharmacosiderite, $KFe_4^{3+}(AsO_4)_3(OH)_4{\cdot}6H_2O$, is an ideal candidate for further investigations of the origin of selectivity in tunnel type network structures from the perspective of bond lengths and coordination number of the cation of interest since it has a closely related structure [9–14]. Ion exchange experiments for the removal of ^{137}Cs and ^{89}Sr have been reported for titanosilicate pharmacosiderite (called TS–P henceforth) and its different substituted forms [16–18]. Synthesis and

*Corresponding author. Fax: +979-845-2370.
E-mail address: clearfield@mail.chem.tamu.edu (A. Clearfield).

0022-4596/$ - see front matter © 2004 Elsevier Inc. All rights reserved.
doi:10.1016/j.jssc.2004.04.042

crystal structure of a rhombohedrally distorted sodium titanium silicate $Na_4(TiO)_4(SiO_4)_3{\cdot}6H_2O$ [15], and a cesium titanium silicate $Cs_3H(TiO)_4(SiO_4)_3{\cdot}4H_2O$, synthesized at high temperature (750°C) and pressure (30,000 psi) with pharmacosiderite topology have also been reported [19].

We pursued two approaches to modify the structure of TS–P in order to modify its ion exchange selectivity. These structural modifications were based on our conclusions on the origins of selectivity in the closely related TS material. In the first approach four titanosilicates with increasing Ge substitution for Si were prepared in order to increase the unit cell dimension of TS–P and thus to modify the position of Cs cations in the channels. Previous studies have indicated that the size of the channels and the hydration environment around the cations influence their position [19,20]. Since the ionic radius of Ge^{4+} (0.40 Å) is larger than Si^{4+} (0.26 Å) in tetrahedral coordination [21], its substitution at the tetrahedral Si site increases the unit cell dimension while its substitution at the octahedral Ti^{4+} (0.605 Å) site reduces it [22]. The substitution at the octahedral site was kept as low as possible via variation in starting gel composition while the substitution at the tetrahedral site was increased so that the fourth sample has complete substitution of Si by Ge (Table 1). In the second approach, similar to the one for TS, we prepared a novel 20% Nb substituted potassium titanosilicate (henceforth called K–NbTS–P) and a germanogermanate (K–GG–P) pharmacosiderite phase and compared their selectivity with a potassium titanosilicate (K–TS–P) phase. The substitution of Nb^{5+} for Ti^{4+} in the framework decreases the amount of charge balancing cations required in the channels and hence can modify ion exchange behavior. In this report the modified ion exchange properties of these phases will be discussed from a structural perspective in light of these changes.

2. Experimental

2.1. Synthesis of pharmacosiderites

Seven pharmacosiderite phases were prepared and were divided in two sets for comparison. The first set consists of four Ti/Ge/Si phases: $HCs_3(TiO)_{3.86}(GeO)_{0.14}(SiO_4)_{2.21}(GeO_4)_{0.82}{\cdot}4H_2O$(Cs–TGSG–P1), $HCs_3(TiO)_{3.72}(GeO)_{0.28}(SiO_4)_{1.53}(GeO_4)_{1.47}{\cdot}4.5H_2$ O(Cs–TGSG–P2), $HCs_3(TiO)_{3.55}$ $(GeO)_{0.45}(SiO_4)_{0.79}$ $(GeO_4)_{2.21}{\cdot}5H_2O$(Cs–TGSG–P3) and $HCs_3(TiO)$ $_{3.55}(GeO)_{0.45}$ $(GeO_4)_3{\cdot}4.5H_2O$(Cs−TGG−P4) that have increasing germanium substitution at the tetrahedral site and were prepared using cesium as the charge compensating counter cations in the channels (Table 1). The second set consists of a Ti/Si; $HK_3Ti_4O_4(SiO_4)_3$ · $4H_2O$ (K–TS–P9), a Ti/Nb/Si; $HK_{2.2}Ti_{3.2}Nb_{0.8}O_4$ $(SiO_4)_3{\cdot}4H_2O$ (K–NbTS–P10) and an all Ge; $Ge_4O_4(GeO_4)_3{\cdot}4H_2O$ (K–GG–P11) phase (Table 2). These three phases were prepared in K-form for the structural studies. The synthetic procedures for the two sets are outlined below. The composition of all the phases was determined by pressed-pellet electron microprobe analysis (EPMA) using a four-spectrometer Cameca S × 50 electron microprobe. The calculation of the chemical compositions of the non-hydrated part, $HCs_xH_{3-x}(TiO)_y(GeO)_{4-y}(SiO_4)_z(GeO_4)_{3-z}$, was based on the fact that Ti occupies only octahedral sites and Si occupies only tetrahedral sites, whereas Ge is distributed between both tetrahedral and octahedral sites in a

Table 1
Summary of gel compositions and reaction products for Cs/Ti/Ge/Si pharmacosiderite phases

Product	Phase	Gel composition	Temp. (°C)	Time (h)
$HCs_3R_1{\cdot}4H_2O$	Cs–TGSG–P1	TiO_2:0.75GeO_2:2.33SiO_2:10.73Cs_2O:240.4 H_2O	200	48
$HCs_3R_2{\cdot}4.5H_2O$	Cs–TGSG–P2	TiO_2:1.40GeO_2:1.59SiO_2:10.53Cs_2O:236.0 H_2O	200	48
$HCs_3R_3{\cdot}5H_2O$	Cs–TGSG–P3	TiO_2:2.05GeO_2:0.66SiO_2:9.74Cs_2O:218.0 H_2O	200	48
$HCs_3R_4{\cdot}4.5H_2O$	Cs–TGG–P4	TiO_2:3.08GeO_2:11.28Cs_2O:252.7 H_2O	200	48

R_1= $(TiO)_{3.86}(GeO)_{0.14}(SiO_4)_{2.21}(GeO_4)_{0.82}$, R_2= $(TiO)_{3.72}(GeO)_{0.28}(SiO_4)_{1.53}(GeO_4)_{1.47}$, R_3= $(TiO)_{3.55}(GeO)_{0.45}(SiO_4)_{0.79}(GeO_4)_{2.21}$, R_4= $(TiO)_{3.55}$ $(GeO)_{0.45}(GeO_4)_3$.

Table 2
Summary of gel compositions and reaction products for K/Ti/Si, K/Ti/Nb/Si and K/Ge pharmacosiderite phases

Product	Phase	Gel composition	Temp. (°C)	Time (h)
HK_3 $R_5{\cdot}4H_2O$	K–TS–P9	1.0TiO_2:4.0 SiO_2:17.5 K_2O:416.0 H_2O	200	168
$HK_{2.2}$ $R_6{\cdot}4H_2O$	K–NbTS–P10	0.8TiO_2:0.1 Nb_2O_5:4.0 SiO_2:17.5K_2O:416.0 H_2O	210	240
HK_3 $R_7{\cdot}4H_2O$	K–GG–P11	1.0GeO_2:13.5KF:138.8H_2O	200	96

R_5= $Ti_4O_4(SiO_4)_3$, R_6= $Ti_{3.2}Nb_{0.8}O_4(SiO_4)_3$, R_7= $Ge_4O_4(GeO_4)_3$.

Table 3
XRD powder data collection and Rietveld refinement results for Ti/Ge/Si pharmacosiderite phases

Phase	Cs–TGSG–P1	Cs–TGSG–P2	Cs–TGSG–P3	Cs–TGG–P4
Composition	$HCs_3R_1 \cdot 4H_2O$	$HCs_3R_2 \cdot 4.5H_2O$	$HCs_3R_3 \cdot 5H_2O$	$HCs_3\ R_4 \cdot 4.5H_2O$
Symmetry/SG	Cubic/$P\bar{4}3m$	Cubic/$P\bar{4}3m$	Cubic/$P\bar{4}3m$	Cubic/$P\bar{4}3m$
Cell constant (Å)	$a = 7.8577(2)$	$a = 7.9000(2)$	$a = 7.9306(2)$	$a = 7.9769(4)$
Volume (Å^3)	485.17(3)	493.05(2)	498.80(4)	507.57(2)
Z	1	1	1	1
Equipment/λ	Bruker-D8/Cu$K\alpha_1$	Bruker-D8/Cu$K\alpha_1$	Bruker-D8/Cu$K\alpha_1$	Bruker-D8/Cu$K\alpha_1$
R_P	0.0791	0.0768	0.0720	0.0848
χ^2	1.885	1.403	1.601	2.019
R_F	0.0904	0.1076	0.0780	0.0918
R_{WP}	0.1019	0.100	0.0867	0.1107
Phase	CsH–TGSG–P5	CsH–TGSG–P6	CsH–TGSG–P7	CsH–TGG–P8
Composition	$H_{3.64}Cs_{0.36}R_1 \cdot 7.2H_2O$	$H_{3.62}Cs_{0.38}R_2 \cdot 7.2H_2O$	$H_{3.59}Cs_{0.41}R_3 \cdot 7H_2O$	$H_{3.65}Cs_{0.35}R_4 \cdot 7.1H_2O$
Symmetry/SG	Cubic/$P\bar{4}3m$	Cubic/$P\bar{4}3m$	Cubic/$P\bar{4}3m$	Cubic/$P\bar{4}3m$
Cell constant (Å)	$a = 7.8773(2)$	$a = 7.9275(2)$	$a = 7.9757(2)$	$a = 8.0237(2)$
Volume (Å^3)	488.80(4)	498.21(3)	507.34(2)	516.57(6)
Z	1	1	1	1
Equipment/λ	Bruker-D8/Cu$K\alpha_1$	Rigaku RU-200/Cu$K\alpha_1$, Cu$K\alpha_2$	Bruker-D8/Cu$K\alpha_1$	Bruker-D8/Cu$K\alpha_1$
R_P	0.0937	0.1028	0.0966	0.1013
χ^2	1.685	2.574	1.847	1.989
R_F	0.1052	0.1127	0.1082	0.1071
R_{WP}	0.1184	0.1293	0.1293	0.1341

$R_1 = (TiO)_{3.86}(GeO)_{0.14}(SiO_4)_{2.21}(GeO_4)_{0.82}$, $R_2 = (TiO)_{3.72}(GeO)_{0.28}(SiO_4)_{1.53}(GeO_4)_{1.47}$, $R_3 = (TiO)_{3.55}(GeO)_{0.45}(SiO_4)_{0.79}(GeO_4)_{2.21}$, $R_4 = (TiO)_{3.55}(GeO)_{0.45}(GeO_4)_3$, SG = Space group.

manner that atomic ratios are equal to the ones obtained from EPMA. The water content was determined by thermogravimetric analysis (TGA) using a TA 950 unit. Finally, all stoichiometries reported in Tables 1–6 were obtained by combining the results of EPMA, TGA, overall charge balance and refined occupancies obtained from Rietveld refinement of models based on X-ray diffraction data.

2.1.1. Synthesis of Cs-forms of germanium substituted pharmacosiderite

The partially Ge substituted Cs-forms of pharmacosiderite were prepared by a technique similar to the one described previously by Behrens et al. [22]. The synthetic procedure began with agitating fumed silica and titanium isopropoxide in doubly deionized (ddi) water in a plastic beaker. The mixture was stirred for 30 min and combined with GeO_2 dissolved in 50% CsOH solution. Four precursors were prepared with compositions shown in Table 1. The mixtures were placed in four 100 mL Teflon lined stainless-steel pressure vessels and heated in an oven at 200°C for 2 days. Highly crystalline solids were filtered off, washed with excess of ddi water and ethanol and dried in an oven at 55°C. Stoichiometric formulas of the products and the composition of the precursors are given in Table 1. The samples were converted to hydrogen forms as described in Section 2.2. below.

2.1.2. Synthesis of K-forms of pharmacosiderites

Synthesis of K–TS–P9: A total of 0.66 mL (6 mmol) of $TiCl_4$ (Alfa Aesar) was mixed with 40 mmol of HCl in ddi water in a plastic beaker. To this solution, 5 mL of 30% H_2O_2 was added under constant stirring followed by 10 mL of 10 M KOH solution and 20 mL of 1.06 M $SiO_2 \cdot nH_2O$ (Fisher) solution in 3 M KOH. The mixture was vigorously stirred for 15 min followed by the addition of 5 mL of 10 M KOH solution. It was placed in a Teflon lined stainless-steel pressure vessel and heated in an oven at 200°C for 7 days.

Synthesis of K–NbTS–P10: A total of 0.34 g (1.25 mmol) of $NbCl_5$ (Aldrich) was mixed with 10 mL of ddi water and 1.4 g of titanium isopropoxide (97%, Alfa Aesar) in a plastic beaker. Similar to the synthesis for K–TS–P, 5 mL of 30% H_2O_2 was added under constant stirring followed by 10 mL of 10 M KOH solution and 20 mL of 1.06 M $SiO_2 \cdot nH_2O$ (Fisher) solution in 3 M KOH. The mixture was sealed and heated in an oven at 210°C for 10 days.

Synthesis of K–GG–P11: Pure germanium pharmacosiderite was synthesized by adding 0.41 g of GeO_2 (Alfa Aesar) to 10 mL of 5.4 M KF solution under constant stirring. To this mixture 6 mL of 0.5 M urea solution was added. The resulting mixture was stirred for 15 min, sealed, and then placed in an oven at 200°C for 4 days.

Products obtained after hydrothermal reaction in each of the above three syntheses were treated likewise: the pressure vessel was cooled to RT; the solid was

Table 4
XRD powder data collection and Rietveld refinement results for Ti/Si, Ti/Nb/Si, all Ge pharmacosiderite phases

Phase	K–TS–P9	K–NbTS–P10	K–GG–P11[a]
Composition	$HK_3R_5 \cdot 4H_2O$	$HK_{2.2}R_6 \cdot 4H_2O$	$HK_3R_7 \cdot 4H_2O$
Symmetry/SG	Cubic/$P\bar{4}3m$	Cubic/$P\bar{4}3m$	Cubic/$I23$
Cell constant (Å)	7.7647(5)	7.7937(2)	15.418(8)
Volume (Å^3)	468.14(5)	473.40(4)	3665.1
Z	1	1	8
Equipment/λ	Bruker-D8/Cu$K\alpha_1$	Bruker-D8/Cu$K\alpha_1$	Single crystal
R_P	0.0907	0.0948	$R = 0.090$
χ^2	6.389	4.684	
R_F	0.1304	0.1403	
R_{WP}	0.1180	0.1216	
Phase	KCs–TS–P12	KCs–NbTS–P13	KCs–GG–P14
Composition	$HCs_{2.8}K_{0.2}R_5 \cdot 5H_2O$	$HCs_{2.1}K_{0.1}R_6 \cdot 5H_2O$	$HCs_{1.77}K_{1.23}\ R_7 \cdot 4H_2O$
Symmetry/SG	Cubic/$P\bar{4}3m$	Cubic/$P\bar{4}3m$	Cubic/$P\bar{4}b2$
Cell constant (Å)	7.8416(3)	7.8622(12)	$a = 10.9311(1)$; $c = 7.7993(1)$
Volume (Å^3)	482.20(2)	486.0(3)	931.94(5)
Z	1	1	2
Equipment/λ	Rigaku RU-200 /Cu$K\alpha_1$, Cu$K\alpha_2$	Bruker-D8/Cu$K\alpha_1$	Rigaku RU-200/Cu$K\alpha_1$,Cu$K\alpha_2$
R_P	0.0999	0.0897	0.0792
χ^2	3.14	1.896	2.356
R_F	0.1125	0.0648	0.1107
R_{WP}	0.1300	0.1092	0.1029

R_5= $Ti_4O_4(SiO_4)_3$, R_6= $Ti_{3.2}Nb_{0.8}O_4(SiO_4)_3$, R_7= $Ge_4O_4(GeO_4)_3$.
[a] Crystallographic data reported by Bialek and Gramlich [11].

Table 5
Refined fractional atomic coordinates, isotropic displacement parameters (Å^2) and occupancies[a] for Cs/Ti/Ge/Si pharmacosiderite phases

Atoms/Site	Phase	Cs–TGSG–P1	Cs–TGSG–P2	Cs–TGSG–P3	Cs–TGG–P4	CsH–TGSG–P5	CsH–TGSG–P6	CsH–TGSG–P7	CsH–TGG–P8
Ti1/Ge1/4(e)	$x = y = z$	0.1435(4)	0.1415(4)	0.1398(4)	0.1402(5)	0.1498(3)	0.1478(3)	0.1458(3)	0.1450(3)
	Occupancy	0.96/0.04	0.93/0.07	0.89/0.11	0.89/0.11	0.96/0.04	0.93/0.07	0.89/0.11	0.89/0.11
	U_{iso} (Å^2)[b]	0.025(1)	0.0231(1)	0.022(1)	0.024(1)	0.025(4)	0.0233(9)	0.0200(9)	0.0207(9)
Ge2/Si1/3(d)	x	0.5	0.5	0.5	0.5	0.5	0.5	0.5	0.5
	$y = z$	0	0	0	0	0	0	0	0
	Occupancy	0.27/0.73	0.49/0.51	0.74/0.26	1	0.27/0.74	0.49/0.51	0.74/0.26	1
O1/ 12(i)	x	0.3844(10)	0.3809(10)	0.3823(10)	0.3769(12)	0.3818(9)	0.3802(10)	0.3794(9)	0.3687(11)
	$y = z$	0.1244(7)	0.1260(7)	0.1253(7)	0.1295(8)	0.1197(9)	0.1216(10)	0.1252(9)	0.1248(9)
O2/ 4(e)	$x = y = \bar{z}$	0.1150(12)	0.1141(9)	0.1083(14)	0.1131(8)	0.1109(12)	0.1125(13)	0.1070(11)	0.1046(11)
Cs1/ 6(g)	$x = y$	0.5	0.5	0.5	0.5	0.5	0.5	0.5	0.5
	z	0.0644(4)	0.0625(4)	0.0559(4)	0.0586(5)	0.0440(20)	0.0518(16)	0.0504(15)	0.0555(15)
	Occupancy	0.5	0.5	0.5	0.5	0.06	0.06	0.07	0.06
	U_{iso} (Å^2)[b]	0.052(2)	0.056(2)	0.055(2)	0.056(2)	0.063(4)	0.049(4)	0.042(4)	0.035(4)
Ow1/4(e)	$x = y = \bar{z}$	0.3424(12)	0.3366(12)	0.3228(11)	0.3321(14)	0.3119(8)	0.3104(9)	0.3076(9)	0.3037(10)
Ow2/1(b)	$x = y = z$		0.5	0.5	0.5	0.5	0.5	0.5	0.5
	Occupancy		0.5	1.0	0.5	0.56	0.62	0.52	0.5
Ow3[c]/6(g)	$x = y$					0.5	0.5	0.5	0.5
	z					0.0440(20)	0.0518(16)	0.0504(15)	0.0555(15)
	Occupancy					0.44	0.44	0.43	0.44

[a] Occupancy = 1 if not reported.
[b] U_{iso} (Å^2) for all the framework atoms (Ti/Ge/Si/O) are set equal to one another as are those for non-framework (Cs/K/Ow) atoms, U_{iso} (Å^2) = $B_{iso}/8\Pi^2$.
[c] Disordered with Cs1.

separated by filtration, rinsed with ddi water and pure ethanol and dried in air at 55°C. Cesium forms of the phases were obtained by ion exchange as described below. Gel composition of the precursors used and stoichiometric formulas of the products obtained are given in Table 2.

2.2. Ion exchange

2.2.1. Preparation of ion exchanged phases for structural investigation

2.2.1.1. Conversion of Cs-form of mixed (Ti/Ge/Si) phases to H-forms. All four Cs phases (Table 1) were

Table 6
Refined fractional atomic coordinates, isotropic displacement parameters (Å^2) and occupancies[a] for Ti/Si and Ti/Nb/Si pharmacosiderite phases

Atoms/Site	Phase	K–TS–P9	K–NbTS–P10	KCs–TS–P12	KCs–NbTS–P13
		A1 = Ti	A1 = Ti/Nb	A1 = Ti	A1 = Ti/Nb
A1/4(*e*)	$x = y = z$	0.1417(2)	0.1415(1)	0.1321(3)	0.138(2)
	Occupancy	1	0.80/0.20	1	0.79/0.21
	U_{iso} (Å^2)[b]	0.0242(10)	0.0415(6)	0.0222(10)	0.029(8)
Si/3(*d*)	x	0.5	0.5	0.5	0.5
	$y = z$	0	0	0	0
O1/12(*i*)	x	0.3778(2)	0.3811(5)	0.3823(8)	0.3793(3)
	$y = z$	0.1235(1)	0.1198(4)	0.1237(5)	0.1233(2)
O2/4(*e*)	$x = y = -z$	0.1120(8)	0.1092(6)	0.1542(10)	0.115(7)
K1[c]/6(*g*)	$x = y$	0.5	0.5	0.5	0.5
	z	0	0	0	0
	Occupancy	1	0.73	0.07	0.03/0.22
	U_{iso} (Å^2)[b]	0.130(4)		0.0332(9)	0.054(9)
Cs1/6(*g*)	$x = y$			0.5	0.5
	z			0.0571(3)	0.078(20)
	Occupancy			0.46	0.24
Ow1/4(*e*)	$x = y$	0.3232(12)	0.3158(7)	0.3297(9)	0.310(7)
	z	0.6768(12)	0.6842(7)	0.6703(9)	0.690(7)
Ow2/4(*e*)	$x = y = z$			0.5	0.5

[a] Occupancy = 1 if not stated.
[b] U_{iso} (Å^2) for all the framework atoms (Ti/Si/Nb/O) are set equal to one another as are those for non-framework (K/Ow) atoms, U_{iso} (Å^2) = $B_{iso}/8\Pi^2$.
[c] Disordered with Cs2 in KCs–NbTS–P13.

converted to the H-form by shaking about 2 g of dry solid with 100 mL of 1 M HNO_3 for 6.5 h. After filtration the solid was again shaken with 100 mL of 0.25 M HNO_3 for 11.5 h. The final product was separated by filtration, washed with ddi water and ethanol and dried in an oven at 55°C. All the cesium was not replaced by the protons and partially exchanged H phases were obtained (Table 3).

2.2.1.2. Conversion of K-form of mixed (Ti/Si, Ti/Nb/Si, all Ge) phases to Cs-forms. Cs-forms (Table 4) were obtained directly by ion-exchange from K-forms (Table 2). Generally, about 0.5 g of dry solid was shaken with 100–130 mL of 0.1 N solution of soluble salt of Cs^+ for 18 h. The solids obtained were separated by filtration, rinsed with ddi H_2O and ethanol and dried in an oven at 55°C. All the potassium was not replaced by cesium cations and partially Cs exchanged phases were obtained (Table 4).

2.2.2. Ion-exchange studies

A batch technique was used to determine the distribution coefficients for Ti/Ge/Si phases. In general, about 40 mg of dry ion exchanger was equilibrated on an orbital shaker with 10 mL of solution for 48 h. The remaining count rate of the filtrate was measured on Wallac 1450 Liquid Scintillation Counter (LSC) and K_d values (mL/g) were calculated using the equation given below.

The three samples in second set (K–TS–P9, K–NbTS–P10 and K–GG–P11) were tested for cesium removal in alkaline simulated solutions. The prepared solution was traced with ^{137}Cs so that the count rate was about 4000–5000 cpm/mL. A total of 100 mL of this solution was introduced to 40 mg of dry ion-exchanger in a 250 mL plastic bottle and agitated on a Barnstead Labline shaker. The suspension was sampled after appropriate periods of time to assess the kinetics of Cs ion removal. The sampled suspension (0.8 mL) was filtered through Millex® 13 mm Syringe Filter with 0.2 μm PVDF (polyvinylidene fluoride) membrane and filtrate (0.5 mL) was counted on LSC. The distribution constant at time t (K_{dt}, mL/g) was calculated using the following equation:

$$K_{dt} = \frac{A_0 - A_t}{A_t} \times \frac{V}{m}, \quad (1)$$

where A_t is the count rate (cpm/mL) of a filtrate at time t, A_0 the initial count rate (cpm/mL), V the total volume of solution (mL), and m the mass of the inorganic ion-exchanger (g).

2.3. X-ray powder diffraction data collection, structure solution, and Rietveld refinement

The samples were packed into a flat plastic or aluminum sample holder and data were acquired in the Bragg–Brentano geometry at RT. Two X-ray

sources were utilized: for some samples a Bruker-D8 advanced computer-automated X-ray diffractometer operating at 40 kV and 40 mA was used and for some others a Rigaku RU-200 automated powder diffractometer operating at 50 kV and 180 mA was used (Tables 3 and 4). Both diffractometers have a copper target. The same step size of 0.02° but count times of 60 and 15 s/step were used in Bruker-D8 and Rigaku, respectively.

In general, powder patterns of most of the synthetic pharmacosiderite phases reported in this study were similar to the ones reported in the literature [9,13,14]. They were indexed using NTREOR which is incorporated in the EXPO suite of programs [23,24]. The solutions which indexed all the peaks corresponded either to cubic cells in some cases or to a tetragonal cell in other (Tables 3 and 4). The powder patterns of several Sr exchanged samples indicated unique peaks that have not been observed in any cubic pharmacosiderite phases. Initial studies and preliminary indexing results indicated that some of these phases were either new or a mixture of two phases. A detailed structural study of the Sr phases will be published elsewhere.

In the beginning of the refinement process each data set was treated individually, using the same general procedure described below. The data were analyzed using the Rietveld technique in conjunction with EXPGUI, the graphical user interface editor for Generalized Structure Analysis System (GSAS) experiment files [25–27]. Atomic positions reported [13,22] for the framework atoms of cubic and tetragonal TS–Ps were used to model and refine the framework cations of the mixed metal TS–Ps reported in this study. In each case the individual site occupancies for the disordered framework Ti/Ge, Ti/Nb and Ge/Si atoms were put equal to the ratio determined from the EPMA and their sum was constrained to a value equal to 1. The positions of Cs^+ and K^+ ions and water molecules in each of the models were obtained from difference Fourier maps, followed by Rietveld refinement of the full patterns. The atomic positions of the framework atoms were refined with soft constraints consisting of bond distances, (Ti/Nb/Ge)–O = 2.00(2) Å for $Ti^{IV}/Nb^{V}/Ge^{IV}$ octahedra, Si–O = 1.63(2) Å for Si tetrahedra and Ge–O = 1.75(2) for Ge tetrahedra. Non-bonded distances of 2.66(2) and 2.85(2) Å were used to constrain O–O atoms in the silicate and germanate tetrahedra, respectively [21]. No bond distance constraints were applied for the refinement of alkali metal cations and water oxygen positions. In all cases, the isotropic thermal parameters for the framework atoms were set equal to one another, as were those for the non-framework cations, with both sets allowed to vary independently during the refinement.

A series of refinements was set up in which the position and occupancy of K^+, Cs^+ and water were examined for all the cases. The process indicated that the non-framework Cs site ($\frac{1}{2}$, $\frac{1}{2}$, z) was half occupied in all the as synthesized Cs phases (Ti/Ge/Si). However, in the H-exchanged forms of Cs phases this site is disordered and occupied by both Cs cations and water molecules. After finding the usual sites for Cs^+ and water molecules, we observed scattering associated with the $\bar{4}3m$ site in the Fourier difference analysis in all H-exchanged (P5–P8) and three Cs (P2–P4) Ti/Ge/Si phases (Tables 3 and 5). This scattering was modeled using water molecules (Ow2) to take into account the stoichiometry previously determined by EPMA and TGA (Tables 3 and 5). In the case of Ti/Nb/Si phases scattering associated with $\bar{4}3m$ was observed only in KCs–TS–P12 and KCs–NbTS–P13 which was also modeled using water molecules (Tables 4 and 6).

During the final cycle of refinement all positional and thermal parameters, profile coefficients, background, unit cell, and diffractometer zero constant were varied. The weight of all soft constraints for bond lengths was reduced gradually to zero. The occupancies of K^+, Cs^+ and water molecules were fixed based on the values calculated from EPMA, TGA, overall charge balance and the obtained refined occupancies. The refinement results showed that the cations and the lattice water molecules in these phases exhibit relatively large thermal parameters, possibly due to disorder or partial occupancy.

Crystallographic data and the results of the individual X-ray data sets with the final positional and thermal parameters for the Cs-form of the Ti/Ge/Si phases are given in Tables 3 and 5. In Tables 4 and 6 similar data is provided for all K-phases except those for the tetragonally distorted KCs–GG–P14 phase, which are provided in Table 11. Selected bond lengths of the framework atoms in TGSG–P1 to P8 and K–TS–P9 to P13 are given Tables 7 and 8, respectively, while Table 12 contains bond lengths of framework atoms in KCs–GG–P14. Selected bond lengths of all the non-framework atoms (Cs–O and K–O) in TGSG–P1 to P8 and K–TS–P9 to P13 are given in Tables 9 and 10. The final observed and calculated diffraction profiles of the Rietveld refinement of only Cs–TGG–P4 and KCs–NbTS–P13 are displayed in Figs. 1 and 2, whereas the ones for TGSG–P1 to P3, KCs–TS–P12, KCs–GG–P14, CsH–TGSG–P5 to P8 and K–TS–P9 to P11 have been submitted to the journal.

3. Results

3.1. Ion-exchange studies

Complications in the remediation of nuclear waste accumulated at the DOE sites results from high alkalinity (up to 1–3 M NaOH) and high ionic strength of the solutions (up to 5–6 M Na^+). The ion-exchange process for the target ion M^+ in the H-form of TS–P

Table 7
Selected interatomic distances (Å) and angles (degrees) in framework atoms of Cs/Ti/Ge/Si pharmacosiderite phases

Phase	Cs–TS–P[a]	Cs–TGSG–P1	Cs–TGSG–P2	Cs–TGSG–P3	Cs–TGG–P4	CsH–TGSG–P5	CsH–TGSG–P6	CsH–TGSG–P7	CsH–TGG–P8
Bond length		A1:Ti1/Ge1	A1:Ti1/Ge1	A1:Ti1/Ge1	A1:Ti1/Ge1	A1:Ti1/Ge1	A1:Ti1/Ge1	A1:Ti1/Ge1	A1:Ti1/Ge1
A1–O1	1.884(5) × 3	1.905(7) × 3	1.900(7) × 3	1.930(7) × 3	1.892(9) × 3	1.858(7) × 3	1.866(8) × 3	1.878(7)	1.810(8)
A1–O2	2.128(4) ×	2.056(6) × 3	2.042(6) × 3	1.999(6) × 3	2.043(7) × 3	2.099(7) × 3	2.102(8) × 3	2.064(6)	2.055(6)
		T: Ge2/Si1	T: Ge2/Si1	T: Ge2/Si1	T: Ge2	T: Ge2/Si1	T: Ge2/Si1	T: Ge2/Si1	T: Ge2
T–O1	1.622(4) × 4	1.654(7) × 4	1.693(7) × 4	1.687(7) × 4	1.760(9) × 4	1.626(8) × 4	1.661(9) × 4	1.708(9)	1.765(9)
Bond angle		A1:Ti1/Ge1	A1:Ti1/Ge1	A1:Ti1/Ge1	A1:Ti1/Ge1	A1:Ti1/Ge1	A1:Ti1/Ge1	A1:Ti1/Ge1	A1:Ti1/Ge1
O1–A1–O1	100.3(2)	98.74)	97.1(4)	96.6(4)	95.0(5)	103.6(4)	102.0(5)	99.6(4)	99.8(5)
O1–A1–O2	87.6(2)	91.2(3)	92.0(3)	93.3(3)	93.2(4)	90.0(5)	90.4(5)	92.9(4)	93.2(4)
O2–A1–O2	83.0(5)	76.9(8)	77.3(8)	74.8(8)	77.3(10)	72.1(6)	73.8(7)	71.6(6)	70.6(7)
O1–A1–O2	167.4(4)	164.7(7)	166.2(7)	165.0(7)	167.7(9)	157.6(4)	160.1(5)	160.6(5)	159.8(6)
Bond angle		T: Ge2/Si1	T: Ge2/Si1	T: Ge2/Si1	T: Ge2	T: Ge2/Si1	T: Ge2/Si1	T: Ge2/Si1	T: Ge2
O1–T–O1	108.8(2)	107.5(3)	107.9(3)	107.8(3)	108.1(3)	109.1(3)	109.06(33)	108.47(28)	110.8(3)
O1–T–O1	110.9(3)	113.4(6)	112.5(6)	112.8(6)	112.2(6)	110.2(6)	110.3(7)	111.5(6)	106.7(6)
Ti1–O1–Si1	132.3(2)	129.7(5)	129.0(5)	128.4(5)	127.5(6)	135.3(7)	133.9(7)	131.4(6)	133.9(6)
Ti1–O2–Ti1	96.6(4)	101.7(6)	101.4(6)	103.3(6)	101.4(8)	105.3(5)	104.1(5)	105.7(4)	104.7(3)

[a] Crystallographic data reported by Behrens et al. [13].

Table 8
Selected interatomic distances (Å) and angles (degrees) in framework atoms of Ti/Si and Ti/Nb/Si pharmacosiderite phases

Phase	K–TS–P9	K–NbTS–P10	KCs–TS–P12	KCs–NbTS–P13
Bond lengths	A1:Ti1; T:Si1	A1:Ti1/Nb1; T:Ge2/Si1	A1:Ti1; T:Ge2	A1:Ti1/Nb1; T:Si1
A1–O1	1.844(2)	1.883(4)	1.964(6)	1.899(14)
A1–O2	1.997(5)	1.987(4)	2.258(8)	2.01(4)
T–O1	1.6554(2)	1.613(4)	1.653(5)	1.667(2)
Bond angles	A1:Ti1; T:Si1	A1:Ti1/Nb1; T:Ge2/Si1	A1:Ti1; T:Ge2	A1:Ti1/Nb1; T:Si1
O1–A1–O1	98.4(1)	99.80(22)	93.79(26)	97.1(10)
O1–A1–O2	91.7(2)	91.48(23)	83.83(21)	91.3(16)
O2–A1–O2	76.0(5)	74.6(3)	98.4(4)	79(4)
O1–A1–O2	164.3(3)	162.3(2)	176.5(4)	167(4)
O1–T–O1	109.18(6)	109.2(2)	108.1(2)	108.89(8)
O1–T–O1	110.06(12)	109.9(4)	112.1(5)	110.6(2)
Ti1–O1–Si1	131.18(13)	132.3(3)	126.7(4)	129.9(8)
Ti1–O2–Ti1	102.4(4)	103.4(2)	80.9(5)	100(4)

Table 9
Selected interatomic distances (Å) and angles (degrees) in Cs/Ti/Ge/Si pharmacosiderite phases

Phase	Cs–TS–P[a]	Cs–TGSG–P1	Cs–TGSG–P2	Cs–TGSG–P3	Cs–TGG–P4	CsH–TGSG–P5	CsH–TGSG–P6	CsH–TGSG–P7	CsH–TGG–P8
Cs1–O1×4	3.143(3)	3.124(5)	3.141(5)	3.163(5)	3.165(6)	3.193(6)	3.195(7)	3.196(6)	3.238(7)
Cs1–O1×4	3.408(2)	3.426(4)	3.440(4)	3.430(4)	3.457(4)	3.392(8)	3.434(7)	3.438(6)	3.502(7)
Average	3.125	3.275	3.290	3.296	3.311	3.292	3.314	3.317	3.37
Cs1–Ow1×2	2.820(2)	2.799(3)	2.831(3)	2.903(3)	2.889(3)	2.974(11)	2.953(9)	2.987(9)	2.988(9)
Cs1–Ow1×2	3.624(3)	3.644(3)	3.643(3)	3.601(3)	3.647(3)	3.500(12)	3.573(10)	3.586(9)	3.642(9)
Average	3.222	3.221	3.237	3.252	3.268	3.237	3.263	3.286	3.315
Cs1–Ow2			3.455(3)	3.522(3)	3.521(4)	3.592(16)	3.553(12)	3.586(12)	3.567(12)

[a] Cs–TS–P = $HCs_3Ti_4O_4(SiO_4)_3 \cdot 4H_2O$; reported by Behrens et al. [13].

can be described by the following reactions:

$$M^+ + \overline{HZ} \rightleftharpoons \overline{MZ} + H^+ \quad (1a)$$

$$H^+ + OH^- \rightleftharpoons H_2O \quad (1b)$$

Reaction (1a) is followed by formation of water: protons, liberated from the ion-exchanger, $\overline{HZ}$, combine with hydroxide ions present in the solution shifting the equilibrium to the products side. Thus, the samples were pretreated with acid and used in H-form for ion exchange experiments.

In the first set of four Ti/Ge/Si phases the K_d values for Cs were measured for the solution consisting of 0.05 M NaOH and 0.05 M $NaNO_3$. The best K_d value

Table 10
Selected interatomic distances (Å) and angles (degrees) in Ti/Si and Ti/Nb/Si pharmacosiderite phases

Atoms	K–TS–P9	K–NbTS–P10	KCs–TS–P12	KCs–NbTS–P13	Atoms	KCs–GG–P14
Cs1–O1 × 4			3.136(4)	3.130(18)	Cs1–O1 × 2	3.277(9)
Cs1–O1 × 4			3.401(3)	3.49(7)	Cs1–O2 × 2	3.183(8)
Cs1–Ow1 × 2			3.573(2)	3.71(13)	Cs1–O4 × 2	3.302(11)
Cs1–Ow1 × 2			2.852(2)	2.79(10)	Cs1–O4 × 2	3.236(10)
Cs1–Ow2			3.473(2)	3.32(16)	Cs1–Ow1 × 2	3.194(9)
Cs2–O1 × 8				3.2574(13)	Cs1–Ow1 × 2	3.400(10)
Cs2–Ow1 × 4				3.225(9)	K1–O1 × 4	3.378(10)
K1–O1 × 8	3.219(9)	3.241(3)	3.240(3)		K1–O2 × 4	2.924(10)
K1–Ow1 × 4	3.172(7)	3.190(7)	3.201(2)		K1– Ow1 × 4	3.036(11)

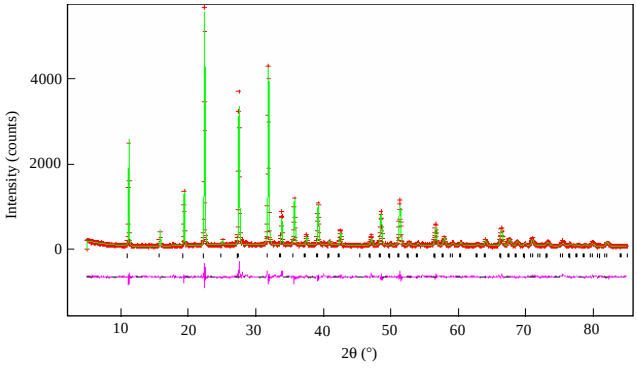

Fig. 1. Observed (+) and calculated (—) X-ray powder diffraction profiles of Cs–TGG–P4 at RT; A difference curve is plotted. Vertical bars mark calculated reflection positions.

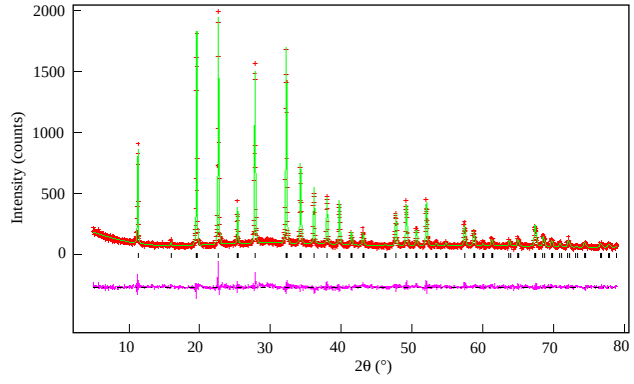

Fig. 2. Observed (+) and calculated (—) X-ray powder diffraction profiles of KCs–NbTS–P13 at RT.

of 4949.8 mL/g after 24 h was observed for the Cs–TGSG–P3 whereas for TGSG–P1 and TGG–P4 it was below 1000 mL/g compared to 1667.3 mL/g for TGSG–P2 (Fig. 3).

The phases in the second set consisting of Ti/Si, Ti/Nb/Si and all Ge were tested in a number of simulants with various compositions. Satisfactory performance was not observed in any of the phases for solutions consisting of 0.015 M KNO_3, 0.00014 M CsCl, and up to 5.6 M Na^+ which closely matches the composition of

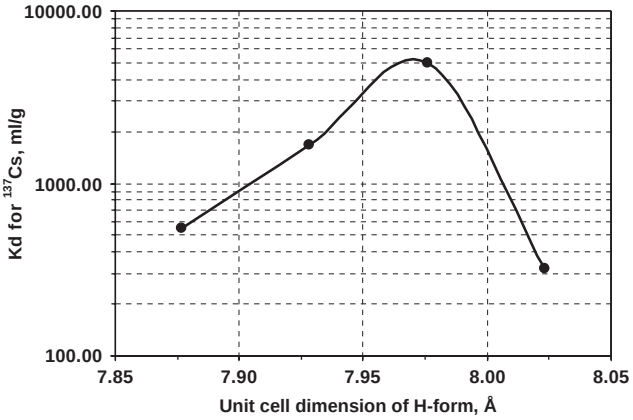

Fig. 3. K_d values for CsH–TGSG–P5, CsH–TGSG–P6, CsH–TGSG–P7, CsH–TGG–P8 as a function of unit cell dimensions. The unit cell dimension increase from phase P5 to P8. Simulant composition: 0.05 M NaOH, 0.05 M $NaNO_3$, ^{137}Cs-trace.

the tank waste at the Savannah River site. No appreciable difference in Cs^+ concentration was observed after 100 mL of such a solution was treated with 40 mg of ion-exchanger for 72 h. However, semi crystalline phases of same compositions show much higher K_d values. Since we were interested in the structural reasons of the origins of selectivity these studies were not included. For a comparative ion-exchange study solutions with lower ionic strength were prepared. In Fig. 4 cesium distribution coefficients for the phases in the second set are plotted against the time of agitation for a solution consisting of 0.05 M NaOH and 0.05 M $NaNO_3$. The plot indicates a better performance by K–NbTS–P10 compared to K–TS–P9 as the cesium K_d values obtained after 24 h for K–NbTS–P10 (16903.7 mL/g) are almost three times higher than K–TS–P9 (5719.3 mL/g). Although higher capacity is observed for K–NbTS–P10, the kinetics of the removal is slower than that in K–TS–P9. There is almost no increase in the K_d values for the non-niobium phase (K–TS–P9) after 3 h of agitation whereas in K–NbTS–P10 it increases by at least 50%. The inferior kinetics of the Nb substituted phase can be explained by slower diffusion

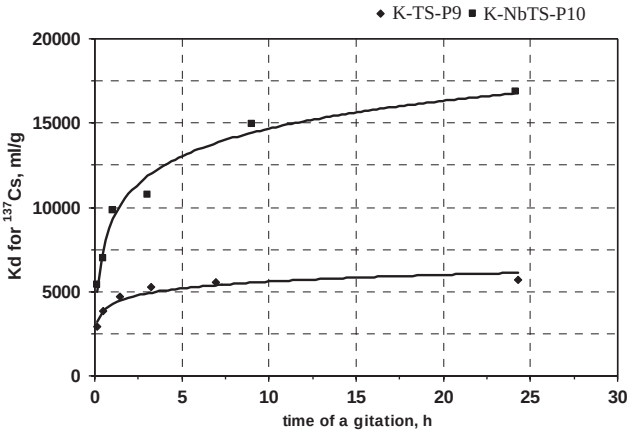

Fig. 4. K_d values for Cs^+ uptake by K–TS–P9 and K–NbTS–P10 as a function of time. Negligible K_d values were observed for K–GG–P11. Simulant composition is similar to the one in Fig. 3. caption.

of Cs to ($\frac{1}{2}$, $\frac{1}{2}$, 0) sites (see discussion). Negligible K_d values (55.5 mL/g after 24 h) were observed in the case of K–GG–P11.

3.2. Structure of various substituted forms: origin of selectivity

General considerations: The structure of TS–P with an ideal formula $HM_3Ti_4O_4(SiO_4)_3 \cdot 4H_2O$ (M = Cs, K, etc.) and having the mineral pharmacosiderite topology has been described in detail previously [9,13]. Generally, TS–P crystallizes in the cubic space group $P\bar{4}3m$ with $a \sim 7.98$ Å. The structure consists of distorted TiO_6 octahedra sharing edges to form a cubane like Ti_4O_4 tetramer and SiO_4 tetrahedra (Figs. 5 and 6). They are connected to each other via the oxygen atom O1 of the silicate groups to form a 3D network of channels. The pore has 8-membered ring (8MR) openings with alternating Si tetrahedra and Ti octahedra. The oxygen atoms O2, which are involved in interconnecting the titanium octahedra, are protonated in the acid form. Each cavity is filled by charge neutralizing extra framework cations that occupy sites in the center of the cube faces such as K^+ ($\frac{1}{2}$, $\frac{1}{2}$, 0) or slightly displaced from the center such as Cs^+ ($\frac{1}{2}$, $\frac{1}{2}$, z) or close to the wall of the spherical cavities such as Sr^{2+} and water molecules (x, x, z) (Figs. 5 and 6). The K cation with a smaller ionic radius than Cs^+ usually occupies sites in the face centers with eight binding sites from silicate oxygen (O1) at ca. 3.234 Å and four binding sites from the water oxygen at ca. 3.169 Å. The Cs cations are disordered in the displaced sites on either side of the ideal face center positions and also have eight binding sites from silicate oxygen but there are two sets of bond lengths; one being shorter of ca. 3.143 Å and other being longer of ca. 3.408 Å. Only two water molecules are bonded to Cs.

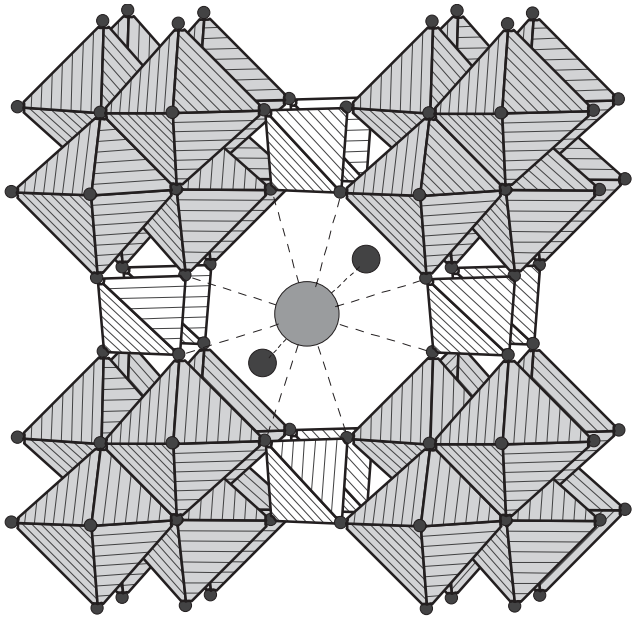

Fig. 5. A polyhedral representation of the crystal structure of pharmacosiderite along [001]. Dark and light gray spheres in the eight ring channel represent water molecules and Cs^+ cations, respectively.

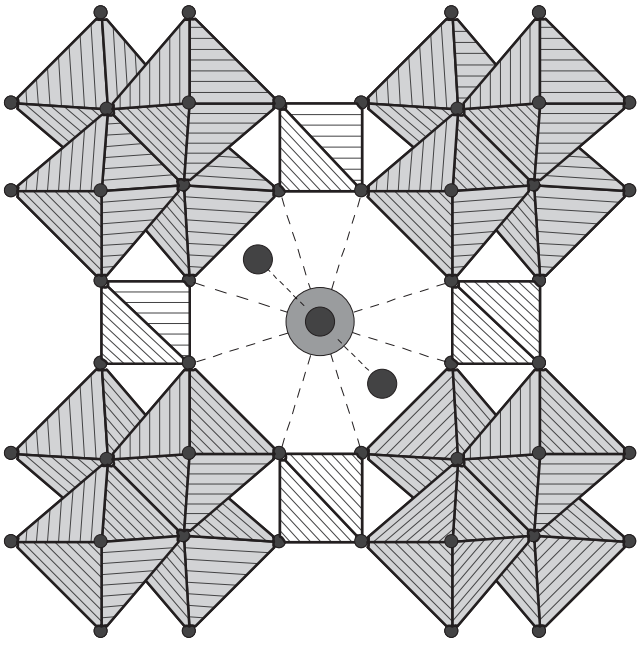

Fig. 6. A polyhedral representation of the crystal structure of substituted pharmacosiderite along [001]. Dark and light gray spheres in the eight ring channel represent water molecules and Cs^+ cations, respectively. Water molecule located above Cs^+ cation at ($\frac{1}{2}$, $\frac{1}{2}$, $\frac{1}{2}$) was observed in some cases.

In the two sets of pharmacosiderite phases described, the octahedra (M) consist of either disordered Ti/Ge (set 1) or Ti/Nb and all Ge atoms (set 2). They are distorted with M–O2 bonds longer than M–O1 bonds in all the as synthesized as well as ion exchanged forms due to the intrinsic nature of the structure with M_4O_4 cubes and

bonding of O2 to the protons. The silicate or germanate tetrahedra display regular bond lengths and angles in all the compounds (Tables 7, 8 and 12).

Ti/Ge/Si phases: The cubic symmetry is retained with the space group $P\bar{4}3m$ (Table 3) in Ti/Ge/Si phases. The Ge substitution increases in both the octahedral Ti site (same for Cs–TGSG–P3 and Cs–TGG–P4) and the tetrahedral Si site with the fourth phase having all Ge in the tetrahedral site (Table 3). Though the substitution of Ti in the octahedral site reduces the lattice parameter, it is offset by an overall increase in the lattice parameter due to a greater Ge substitution in the tetrahedral Si site. The unit cell dimension increases by 0.12 Å and the diameter of the spherical 8MR opening by 0.048 Å from Cs–TGSG–P1 to Cs–TGG–P4 (Table 3). The swelling of the channel results in the displacement of the Cs cation by as much as 0.0085 Å along the *z*-axis towards the ideal site $(\frac{1}{2}, \frac{1}{2}, 0)$ in the case of Cs–TGSG–P3. Despite having the largest unit cell dimension Cs cations are not closest to the ideal site in Cs–TGG–P4 possibly due to interaction with water molecules. The disordered Cs cations are statistically at 50% occupancy at the 2 mm site in all four phases. In Cs–TGSG–P2, Cs–TGSG–P3 and Cs–TGG–P4, a water molecule (Ow2) with variable occupancy was also located at the center of the unit cell $(\frac{1}{2}, \frac{1}{2}, \frac{1}{2})$ with site symmetry $\bar{4}3m$ besides the usual site for water (Ow1) at 3 m $(x, x, \bar{z})$ (Table 5). In Cs–TGSG–P1 an attempt to place a water molecule at the $\bar{4}3m$ site resulted in unrealistically close contact (2.14(3) Å) with a fully occupied water site (Ow1). Water contents in all the phases were derived from TGA studies in conjunction with refined occupancy obtained via the Rietveld refinement. Thus the Cs cation has different coordination environments in the four phases. In Cs–TGSG–P1, Cs1 has eight binding sites with framework oxygen (O1) and two with water molecules (Ow1) resulting in the usual ten coordinate complex. In Cs–TGSG–P2, Cs–TGSG–P3 and Cs–TGG–P4, it has eight binding sites with O1, two with Ow1 and one with a half (Cs–TGSG–P2 and Cs–TGG–P4) or fully (Cs–TGSG–P3) occupied Ow2 which results in an 11 coordinate complex for Cs–TGSG–P3 and a variable coordination between 10 and 11 for Cs–TGSG–P2 and Cs–TGG–P4. The average Cs–O1 bond lengths are 3.275, 3.290, 3.296, 3.311 Å and average Cs–Ow1 bond lengths are 3.221, 3.237, 3.252 and 3.268 Å in Cs–TGSG–P1 to P4, respectively (Table 9). Clearfield et al. [13] reported average Cs–O1 and Cs–Ow1 bond lengths of 3.125 Å and 3.222 Å, respectively in the non-substituted titanosilicate, $HCs_3Ti_4O_4(SiO_4)_3 \cdot 4H_2O$ (Cs–TS–P, Table 9). The Ti–O2–Ti bond angles in the Ti_4O_{16} clusters are more stretched (Table 7) compared with the Cs–TS–P. The maximum stretch was observed in the Cs–TGSG–P3 which has the highest K_d values.

The as-synthesized Cs-forms were converted to H-forms for Cs uptake studies. However, all Cs could not be exchanged for protons without destroying the structure in these compounds. Further, highly crystalline, mixed Ti/Ge/Si phases suitable for structural

Table 11
Refined fractional atomic coordinates and isotropic displacement parameters (Å^2) for KCs–GG–P14

Atom	Site	*x*	*y*	*z*	U_{iso} [a]
Ge1	8*i*	0.1379(2)	−0.0063(2)	0.1399(3)	0.0175(4)
Ge2	4*g*	0.2670(1)	0.2329(1)	0	0.0175(4)
Ge3	2*c*	0	0	0.5	0.0175(4)
O1	8*i*	0.1431(6)	0.2458(8)	−0.1428(10)	0.0175(4)
O2	8*i*	0.2671(9)	0.0990(5)	0.1218(10)	0.0175(4)
O3	8*i*	0.1054(8)	−0.0204(12)	−0.1055(11)	0.0175(4)
O4	8*i*	−0.1264(3)	0.0194(11)	0.3676(5)	0.0175(4)
Cs1	4*h*	0.2955(1)	0.2045(1)	0.5	0.0402(6)
K1	2*b*	0.5	0	0	0.0402(6)
Ow1	8*i*	0.3376(10)	−0.0501(8)	0.6921(13)	0.0402(6)

Occupancy of all atoms = 1, crystallographic details in Table 4.
[a] U_{iso} (Å^2) for all the framework atoms (Ge/O) are set equal to one another as are those for non-framework (K/Cs/Ow) atoms.

Table 12
Selected interatomic distances (Å) and angles (degrees) in KCs–GG–P14

Atom	Bond length	Atom	Angle	Atom	Angle	Atom	Angle
Ge1–O1	1.904(7)	O1–Ge1–O2	91.0(4)	O3–Ge1–O4	91.6(4)	Ge1–O1–Ge2	99.1(5)
Ge1–O2	1.828(8)	O1–Ge1–O3	93.6(5)	O3–Ge1–O4	98.8(4)	Ge1–O1–Ge2	103.0(4)
Ge1–O3	1.953(9)	O1–Ge1–O3	96.2(4)	O1–Ge2–O1	106.1(7)	Ge1–O1–Ge2	129.54(23)
Ge1–O3	2.059(13)	O1–Ge1–O4	88.2(4)	O1–Ge2–O2	114.3(4)		
Ge1–O3	1.793(11)	O1–Ge1–O3	168.6(4)	O1–Ge2–O2	107.5(4)		
Ge1–O3	1.786(5)	O2–Ge1–O3	96.6(4)	O2–Ge2–O2	107.2(7)		
Mean		O2–Ge1–O3	166.09(35)	O4–Ge3–O4	110.65(13)		
Ge2–O1	1.760(4) × 2	O2–Ge1–O3	96.5(4)	O4–Ge3–O4	107.13(26)		
Ge2–O2	1.745(4) × 2	O2–Ge1–O4	100.5(4)	O4–Ge3–O4	110.65(13)		
Mean		O3–Ge1–O3	71.2(4)	Ge1–O1–Ge2	123.2(4)		
Ge3–O4	1.739(4) × 4	O3–Ge1–O3	77.1(5)	Ge1–O2–Ge2	124.8(5)		
		O3–Ge1–O3	74.7(4)	Ge1–O3–Ge1	109.1(5)		

studies could not be synthesized in the K-form. The H-exchanged samples also indicated an increase of 0.146 Å in the unit cell dimension from CsH–TGSG–P5 to P8 while retaining the cubic symmetry and the space group, $P\bar{4}3m$ (Table 3). Each of the unit cell dimensions in the H-form samples is larger than the corresponding Cs-form due to an increase in hydration level. The Cs cations are disordered with water molecules, Ow3, at $(\frac{1}{2}, \frac{1}{2}, z)$ (Table 5). Water molecules (Ow2) with variable occupancy were also located at the center of the unit cell $(\frac{1}{2}, \frac{1}{2}, \frac{1}{2})$ besides the usual site for water (Ow1) at $3m$ $(x, x, \bar{z})$. Unlike in the case of Cs–TGSG–P1, a water molecule was located at $(\frac{1}{2}, \frac{1}{2}, \frac{1}{2})$ in CsH–TGSG–P1 (Table 5).

Ti/Si, Ti/Nb/Si and pure Ge phases: In the second comparative study a 20% niobium substituted titanosilicate pharmacosiderite (K–NbTS–P10) phase was prepared in K-form and its Cs^+ exchange capacity was compared with a titanosilicate (K–TS–P9) and germanium germanate (K–GG–P11). The K–GG–P11 crystallizes in the body-centered cubic supercell, defined in $I23$ ($a \sim 15.42$ Å). The crystal structure of a similar pure germanium phase has been reported [11,14]. In K–TS–P9 and K–NbTS–P10, a 12 coordinate K was observed with eight equal binding sites from framework oxygens (O1) and four equal binding sites from water molecules (Ow1) (Table 8). There are two different disordered K sites in K–GG–P11 that have 12 and 10 coordination with framework oxygen atoms and water molecules [11].

The K-forms were converted directly to partial Cs forms via ion exchange. The exchanged KCs–GG–P14 phase has a unit cell with tetragonal symmetry which is related to the cubic cell by the relationship; $a_t = \sqrt{2}a_c$ and $c_t = c_c$ (the subscript t and c denote tetragonal and cubic cells, respectively). In the reduced symmetry cell, Cs cations occupy site $(\bar{x}, \bar{x}+\frac{1}{2}, \frac{1}{2})$ while K cations occupy site $(\frac{1}{2}, 0, 0)$. Both the K and Cs cations form 12 coordinate complexes that include six bonds with framework oxygen and six bonds with water in the Cs complex and eight bonds with framework oxygen and four bonds with water in the K complex. Potassium cations also form a 12 coordinate complex in KCs–NbTS–P13 and KCs–TS–P12, however, they are disordered with Cs cations in KCs–NbTS–P13. The average K–O and Cs–O bond lengths are 3.167 and 3.175 Å (Table 10). There is only one independent site for water in KCs–GG–P14 (Table 11) while two sites for water are observed in KCs–TS–P12 and KCs–NbTS–P13 (Table 6).

4. Discussion

In order to modify the selectivity of pharmacosiderite for Cs we pursued two approaches based on our prior studies in a closely related material with sitinakite topology [5]. In the first approach, the size of the spherical 8MR was increased in a systematic way by modifying the gel composition so that the substitution of Ge for Si in the tetrahedral site is maximized and its substitution for Ti in the octahedral site is kept to a minimum possible.

The K_d values for ^{137}Cs uptake from the partially H-exchanged samples indicated an increasing trend, 553.22, 1667.27 and 4949.83 mL/g, along with the unit cell dimensions up to the third phase (Cs–TGSG–P3) only (Fig. 3). However, the K_d value was only 320.14 mL/g for Cs–TGG–P4. The crystal structure of Cs–TGSG–P3 revealed that Cs approaches closest $(\frac{1}{2}, \frac{1}{2}, 0.0559(4))$to the ideal position $(\frac{1}{2}, \frac{1}{2}, 0)$ as shown in Fig. 7. This position is more symmetrical compared to the other three phases in terms of Cs–O1 bonding distances. The two sets of four Cs–O1 bonds and two sets of two Cs–Ow1 are closest to each other (Table 9). It can be remembered that in the ideal site for Cs, the eight bonds to framework oxygen atoms and the four bonds to water oxygen are equal. However, we believe that it is the difference in the coordination environment around Cs that results in the different ion exchange behavior of these materials. In Cs–TGSG–P1, there are four water molecules per formula unit resulting in a 10 coordinate Cs complex with eight bonds to O1 and two bonds to Ow1 for each of the split positions of Cs1. While in Cs–TGSG–P3, there is an additional fully occupied water at $(\frac{1}{2}, \frac{1}{2}, \frac{1}{2})$ resulting in an eleven coordinate Cs complex. In Cs–TGSG–P2 and Cs–TGG–P4, this $\bar{4}3m$ site is only half occupied thus a coordination number between 10 and 11 can be assumed for the Cs cation in these two phases. The observed K_d are consistent with observed coordination numbers.

In the second approach, a 20% Nb substituted phase was prepared and its K_d values were compared with a pure Ge and TiSi phases. Our previous studies on the

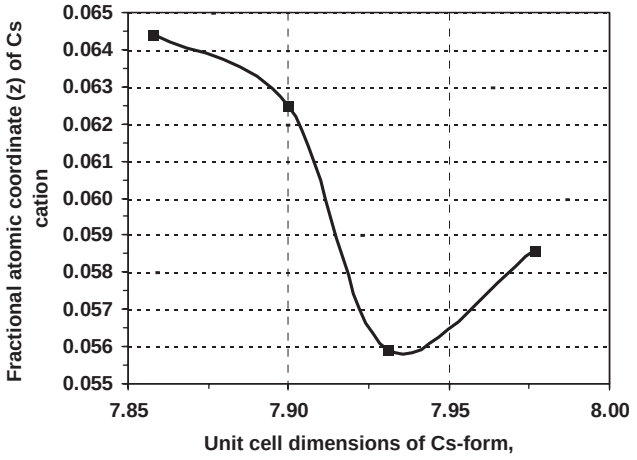

Fig. 7. Fractional atomic coordinate, z (site = 6 g) of Cs cation for Cs–TGSG–P1, Cs–TGSG–P2, Cs–TGSG–P3, Cs–TGG–P4 as a function of unit cell dimension of the phases.

closely related structure of the 25% Nb substituted titanosilicate with sitinakite topology showed that the population of water vs. Na^+ in the channel adjusts to charge-balance the $Nb^{5+} \rightleftharpoons Ti^{4+}$ substitution. This in turn modifies the coordination environment of Cs and hence its uptake by the exchanger. Higher K_d values (16903.71 mL/g after 24 h) for Cs uptake were indeed observed for KCs–NbTS–P13 compared to KCs–TS–P12 (5719.32 mL/g after 24 h) while KCs–GG–P14 showed negligible K_d values (55.50 mL/g after 24 h). No change in Cs coordination number was observed for KCs–NbTS–P13. Since K cations occupy the ideal site $(\frac{1}{2}, \frac{1}{2}, 0)$ in the center of spherical 8MR in K–TS–P9, they could not be completely exchanged for Cs cations unlike the loosely fitting Na ions in the case of sitinakite which occupy sites close to the walls of the 8MR. The Nb substitution, therefore only results in a decrease in K occupancy at $(\frac{1}{2}, \frac{1}{2}, 0)$ and a stable model was obtained with disordered Cs/K cations at this site. Thus some Cs cations can be accommodated in the K sites due to a decrease in K cations in KCs–NbTS–P13. The slow kinetics observed in KCs–NbTS–P13 can be correlated to slow migration of Cs cations to $(\frac{1}{2}, \frac{1}{2}, 0)$ site once they occupy $(\frac{1}{2}, \frac{1}{2}, z)$. In KCs–TS–P12, the refinement became unstable with disordered Cs/K model. Negligible K_d values obtained in KCs–GG–P14 can be correlated to the ideally placed K1 cations that tightly fit in the 4 h sites in the smallest 8MRs. In fact the negligible K_d values observed for this phase makes it an excellent candidate for K removal from tank waste simulants in the H-form. Among all the as synthesized K forms shortest K–O distances of 2.924 (10) Å were observed in KCs–GG–P14 (Table 10). In this phase Cs cations partially occupy sites with symmetry 2*b* to compensate for charge balance.

Structural studies and K_d values of Sr exchange phases have not been included in this work. We observed either a phase change or mixture of phases upon Sr exchange in some of the phases. A detailed study will be published elsewhere.

5. Conclusions

We synthesized a range of compositions with pharmacosiderite topology and studied their ion exchange properties. The origin of selectivity for Cs^+ cations in these phases has been correlated with the atomic structure. In the first set of mixed Ti/Ge/Si phases, the size of the eight ring was systematically increased in order to shift the Cs cation as close as possible to the ideal site $(\frac{1}{2}, \frac{1}{2}, 0)$ that is usually occupied by the smaller K cations. This Cs movement in turn shifts the position of water molecules (Ow1) allowing enough space in the center of the channel $(\frac{1}{2}, \frac{1}{2}, \frac{1}{2})$ for another half (in Cs–TGSG–P2 and P4) or fully (in Cs–TGSG–P3) occupied water molecule (Ow2) to move in. The highest K_d values were observed in the phase that has Cs ion closest to the ideal site which results in the highest coordination number resulting from an additional water molecule at $(\frac{1}{2}, \frac{1}{2}, \frac{1}{2})$. In Cs–TGG–P1, Cs ion farthest from the ideal site and no additional water molecule was observed at $(\frac{1}{2}, \frac{1}{2}, \frac{1}{2})$. This site is too close to the fully occupied site with Ow1. In Nb-substituted TiSi phase, better K_d values can be correlated to the decrease in charge balance requirement in the channels resulting from the substitution of Nb^v for Ti^{iv}. Disordered of Cs cations were observed in the ideal site $(\frac{1}{2}, \frac{1}{2}, 0)$ along with K besides the usual site $(\frac{1}{2}, \frac{1}{2}, z)$ in contrast to the non-Nb Ti/Si phase. The pure Ge phase appears to be the best K sorbent as it has shortest K–O distances and does not show ion exchange behavior under ordinary conditions. In general, it is difficult to remove the cations from the K-form of TiSi phase as they 'plug up' well in the ideal site with eight equal bonds with framework oxygen and four equal bonds with water molecules compared to the 'rattling' Na cations in the titanosilicate with the sitinakite topology.

Acknowledgments

We thankfully acknowledge the US Department of Energy, Environmental Management Science Program, Grant No. DE-FG07-01ER6300 with funds supplied through Westinghouse Savannah River Company for support of this study.

References

[1] A. Clearfield, Inorganic Ion Exchange Materials, CRC Press, Boca Raton, FL, 1982.
[2] P. Sylvester, E.A. Behrens, G.M. Graziano, A. Clearfield, Sep. Sci. Technol. 34 (1999) 1981.
[3] A.I. Bortun, L.N. Bortun, D.M. Poojary, O. Xiang, A. Clearfield, Chem. Mater. 12 (2000) 294.
[4] T. Moller, R. Harjula, Sep. Sci. Technol. 36 (2001) 885.
[5] A. Tripathi, D.G. Medvedev, M. Nyman, A. Clearfield, J. Solid State Chem. 175 (2003) 72.
[6] R.G. Anthony, R. G. Dosch, C.V. Philip, WO9419277.
[7] D.M. Poojary, R.A. Cahill, A. Clearfield, Chem. Mater. 6 (1994) 2364.
[8] W.R. Wilmarth, D.D. Walker, F.F. Fondeur, S.D. Fink, M. Nyman, J. Krumhansl, J.T. Mills, V.H. Dukes, B.H. Croy, WSRC-TR. (2001) 00221.
[9] M.J. Buerger, W.A. Dollase, I. Garaycochea-Wittke, Z. Kristallogr. 125 (1967) 92.
[10] D.M. Chapman, A.L. Roe, Zeolites 10 (1990) 730.
[11] R. Bialek, V. Gramlich, Z. Kristallogr. 198 (1992) 67.
[12] T.M. Nenoff, W.T.A. Harrison, G.D. Stucky, Chem. Mater. 6 (1994) 525.
[13] E.A. Behrens, D.M. Poojary, A. Clearfield, Chem. Mater. 8 (1996) 1236.
[14] M.A. Roberts, A.N. Fitch, Z. Kristallogr. 211 (1996) 378.

[15] M.S. Dadachov, W.T.A. Harrison, J. Solid State Chem. 134 (1997) 409.
[16] P. Sylvester, A. Clearfield, Solvent Extraction Ion Exchange 16 (1998) 1527.
[17] A. Dyer, M. Pillinger, S. Amin, J. Mater. Chem. 9 (1999) 2481.
[18] A.M. Puziy, J.R. Garcia, J. Radioanal. Nucl. Chem. 240 (1999) 851.
[19] W.T.A. Harrison, T.E. Gier, G.D. Stucky, Zeolites 15 (1995) 408.
[20] A. Clearfield, Solid State Sci. 3 (2001) 103.
[21] R.D. Shannon, C.T. Prewitt, Acta Crystallogr. B: Struct. Crystallogr. Cryst. Chem. 25 (1969) 925.
[22] E.A. Behrens, D.M. Poojary, A. Clearfield, Chem. Mater. 10 (1998) 2575.
[23] A. Altomare, J. Foadi, C. Giacovazzo, A.G.G. Moliterni, M.C. Burla, G. Polidori, J. Appl. Crystallogr. 31 (1998) 74.
[24] A. Altomare, C. Giacovazzo, A. Guagliardi, A.G.G. Moliterni, R. Rizzi, P.-E. Werner, J. Appl. Crystallogr. 33 (2000) 1180.
[25] H.M. Rietveld, Acta Crystallogr. 22 (1967) 151.
[26] A.C. Larson, R.B. Von Dreele, Generalized Structure Analysis System (GSAS), MS-H805, Los Alamos, NM 87545, 1990.
[27] B.H. Toby, J. Appl. Crystallogr. 34 (2001) 210.